

2-28-2020

Salt marsh monitoring along the mid-Atlantic coast by Google Earth Engine enabled time series

Anthony D. Campbell

Yeqiao Wang

RESEARCH ARTICLE

Salt marsh monitoring along the mid-Atlantic coast by Google Earth Engine enabled time series

Anthony Daniel Campbell¹✉, Yeqiao Wang*

Department of Natural Resources Science, University of Rhode Island Kingston, Kingston, Rhode Island, United States of America

✉ Current address: Currently at the Yale School of Forestry & Environmental Studies, New Haven, Connecticut, United States of America

* yqwang@uri.edu

OPEN ACCESS

Citation: Campbell AD, Wang Y (2020) Salt marsh monitoring along the mid-Atlantic coast by Google Earth Engine enabled time series. PLoS ONE 15(2): e0229605. <https://doi.org/10.1371/journal.pone.0229605>

Editor: Changshan Wu, University of Wisconsin Milwaukee, UNITED STATES

Received: September 11, 2019

Accepted: February 10, 2020

Published: February 28, 2020

Copyright: © 2020 Campbell, Wang. This is an open access article distributed under the terms of the [Creative Commons Attribution License](https://creativecommons.org/licenses/by/4.0/), which permits unrestricted use, distribution, and reproduction in any medium, provided the original author and source are credited.

Data Availability Statement: All aboveground green biomass trend rasters are available from the figshare database ([10.6084/m9.figshare.11440968](https://doi.org/10.6084/m9.figshare.11440968)). The binary classification of salt marsh for Assateague Island derived from Worldview-2 is also available from the figshare database ([10.6084/m9.figshare.11440968](https://doi.org/10.6084/m9.figshare.11440968)). The underlying Landsat tier 1 surface reflectance data are available on Google Earth Engine provided by U.S. Geological Survey (https://developers.google.com/earth-engine/datasets/catalog/LANDSAT_LC08_C01_T1_SR) and the National Wetland Inventory was provided by U.S. Fish and Wildlife Service

Abstract

Salt marshes provide a bulwark against sea-level rise (SLR), an interface between aquatic and terrestrial habitats, important nursery grounds for many species, a buffer against extreme storm impacts, and vast blue carbon repositories. However, salt marshes are at risk of loss from a variety of stressors such as SLR, nutrient enrichment, sediment deficits, herbivory, and anthropogenic disturbances. Determining the dynamics of salt marsh change with remote sensing requires high temporal resolution due to the spectral variability caused by disturbance, tides, and seasonality. Time series analysis of salt marshes can broaden our understanding of these changing environments. This study analyzed aboveground green biomass (AGB) in seven mid-Atlantic Hydrological Unit Code 8 (HUC-8) watersheds. The study revealed that the Eastern Lower Delmarva watershed had the highest average loss and the largest net reduction in salt marsh AGB from 1999–2018. The study developed a method that used Google Earth Engine (GEE) enabled time series of the Landsat archive for regional analysis of salt marsh change and identified at-risk watersheds and salt marshes providing insight into the resilience and management of these ecosystems. The time series were filtered by cloud cover and the Tidal Marsh Inundation Index (TMII). The combination of GEE enabled Landsat time series, and TMII filtering demonstrated a promising method for historic assessment and continued monitoring of salt marsh dynamics.

Introduction

Drivers of salt marsh loss are diverse from direct anthropogenic disturbances such as reclamation for agriculture [1], and indirect factors such as replacement by mangroves [2,3], eutrophication [4], herbivory [5,6], and sea-level rise (SLR) [7, 8, 9]. For example, less than half of salt marshes are predicted to keep pace with projected SLR under the Intergovernmental Panel on Climate Change's (IPCC) representative concentration pathway 2.6, which assumes significant reductions of CO₂ emissions [10]. The mid-Atlantic coast is one region where accretion is unlikely to keep pace due in part to high projected rates of SLR [11], glacial isostatic adjustment, and anthropogenic processes [12].

(<https://www.fws.gov/wetlands/data/Mapper.html>). Additional training and testing data were utilized and are available from U.S. Geological Survey (<https://www.sciencebase.gov/catalog/item/5a0c7b04e4b09af898cd401c>) [52] and the Environmental Data Initiative (<https://doi.org/10.6073/pasta/44051c788e3bb5339b20a0ce9307d992>).

Funding: Y.W. received funding from the National Park Service as part of grant number: NPS_P14AC00230. The funding organization website can be found at <https://www.nps.gov/index.htm>. Y.W. also received publication support from the Environmental Data Center at the University of Rhode Island funding organizations website can be found at <https://www.edc.uri.edu/>. A.D.C. received support from the NASA RI Space Grant. Funding organization website can be found at <https://www.brown.edu/initiatives/ri-space-grant/>. A.D.C. also received data access to in situ biomass estimates from the Virginia Coast Reserve Long-Term Ecological Research with support of NSF Grants BSR-8702333-06, DEB-9211772, DEB-9411974, DEB-0080381, DEB-0621014 and DEB-1237733. The organizations website can be found at <https://www.vcrlter.virginia.edu/home2/>. The funders had no role in study design, data collection and analysis, decision to publish, or preparation of the manuscript.

Competing interests: The authors have declared that no competing interests exist.

The current and future response of salt marsh to SLR is uncertain. Recent estimates of salt marsh change have shown a slowing of loss across the Atlantic coast of the USA from 2004 to 2009 with a 0.4% reduction of estuarine emergent vegetation [13]. In contrast, estimates from specific sites have demonstrated extensive losses of salt marsh including Rhode Island, Jamaica Bay, and the Chesapeake Bay [7,14,15]. Recent projections of salt marsh change suggest salt marshes will expand if they can migrate into the uplands unimpeded by coastal development [16]. Anthropogenic action or inaction contributes to the uncertainty of the projections which, necessitates monitoring of salt marsh to identify areas of loss. *In situ* methods for monitoring salt marsh have limited ability to understand regional and global salt marsh trends or verify salt marsh models. Time series analysis of satellite remote sensing has appropriate spatial and temporal resolution to monitor and understand salt marsh change.

In the mid-Atlantic, SLR is exceeding accretion rates at many locations [10]. The characteristics of these salt marshes makes them the equivalent of canaries in the coal mine; ideal systems for studying and monitoring the effect of SLR on salt marsh resilience. Many mid-Atlantic salt marshes have microtidal ranges and low sediment budgets. These characteristics increase the risk of loss to SLR [17]. The limited sediment supply of the mid-Atlantic coastal salt marshes, composed predominantly of *S. alterniflora* or *S. patens*, results in peat dominated wetlands [18], i.e., salt marshes which rely primarily on organic matter to build elevation, as opposed to those along the southeast U.S. coast, which accrete mostly mineral material [19]. Peat dominated salt marshes adapt more slowly to SLR [20]. Mid-Atlantic salt marsh characteristics such as tidal range, soil material, subsidence, and human disturbance, elevate the risk of SLR to the regions salt marsh.

A variety of remote sensing data have been applied to evaluate wetland change including very high-resolution (VHR) satellite imagery [21], Landsat [22], Synthetic Aperture Radar (SAR) [23], and aerial imagery [7]. Time series analysis of salt marshes has been conducted with many sensors including the Moderate Resolution Imaging Spectroradiometer (MODIS) [24], SPOT-5 [25], and the Landsat archive [26,27]. Google Earth Engine (GEE) has enabled time series, analysis in freshwater wetland change analysis [28]. Cloud computing and High-Power Computing are frequently employed in time series studies to quantify ecological processes, and land cover land use change (LCLUC) [29–31]. GEE facilitates our ability to understand LCLUC at regional and global scales. The utilization of these methods in salt marsh landscapes can further clarify how and where these ecosystems are changing.

Remote sensing of salt marsh is prone to time series outliers due to tidal inundation, extreme water events, and atmospheric anomalies. The tidal stage at the time of image acquisition can directly impact the extent of salt marsh vegetation in Landsat imagery [32] and VHR imagery at high tide when portions of the low marsh are submerged [21]. Time series outliers can alter the attributes and the results of an analysis [33]. Therefore, the effect of tidal outliers is a concern in remote sensing of salt marsh. The tidal marsh inundation index (TMII) has been successfully used to identify inundated pixels and improve time series results for MODIS [34]. Season and trend decomposition of the time series is another way to minimize the effect of outliers, the method is robust to noise when detecting changes greater than 0.1 Normalized Difference Vegetation Index (NDVI) [35]. In this study, filtering and seasonal and trend decomposition mitigated the effect of tidal inundation on the time series. This study innovates by applying a time series approach to aboveground green biomass (AGB) estimates derived from remote sensing to clarify long-term change of the salt marsh at a regional scope.

This study explores the capacity of time series analysis to help understand salt marsh dynamics in association with locations of stability, gradual loss, change driven by disturbance, or a combination of loss and recovery and the sources of change such as interior drowning, edge erosion, barrier island migration processes, and shifts in vegetation composition. The

objectives of this study include: (1) to evaluate the salt marsh AGB estimates with high spatial resolution imagery and *in situ* biomass samples; (2) to model the change in AGB of mid-Atlantic salt marshes from 1999 to 2018 and (3) to test the TMII for use with GEE enabled Landsat time series.

Methods

Study site

The mid-Atlantic coastal region has a variety of estuaries and bays including drowned river valleys such as the Chesapeake and Delaware Bays and barrier island lagoon systems such as Great South Bay and Barnegat Bay. Watersheds were used as the spatial extents for this study because salt marshes are affected by their watershed's sediment supply [36] and nutrient loads [4]. The study selected USGS Hydrological Unit Code 8 (HUC-8) watersheds. This study, covered coastal watersheds across the southern sections of Long Island, NY, New Jersey, Delaware, Maryland, Virginia, and northern North Carolina (Fig 1). The majority of these watersheds are dominated by back-barrier lagoon systems with extensive salt marshes. The exception was the Tangier watershed within the Chesapeake Bay which is a drowned river valley. The Tangier watershed is an area of extensive land loss due to SLR, low sediment load, and groundwater withdrawal [22]. The dominant salt marsh species in these watersheds are *S. alterniflora* in the low marsh and *Juncus gerardii*, *S. patens*, *Distichlis spicata*, and *J. roemerianus* in the high marsh. Extensive changes in the mid-Atlantic are projected from climate change including shifts in salt marsh plant composition and extent, displacement of species [37], increases in decomposition rates leading to a reduction of organic accretion in the low marsh [38], and possible reductions in belowground biomass due to earlier senescence of *S. alterniflora* [39].

Data

Landsat 7 and Landsat 8 Tier-1 imagery accessible with GEE were used for the time series analysis. Multispectral Landsat 7 Enhanced Thematic Mapper + (ETM+) has a 30 m spatial resolution for bands 1–5 and 7. The panchromatic band 8 has a 15 m spatial resolution. Landsat 8 Operational Land Imager (OLI) has a 30 m spatial resolution for bands 1–7 and 9. The OLI panchromatic band 8 has the same 15 m spatial resolution as the ETM+ panchromatic band.

The selected ETM+ imageries were acquired from 7/01/1999 to 4/01/2017. The OLI imageries were acquired 3/20/2013–7/28/2018. The HUC-8 watersheds are covered by Landsat scenes of WRS-2 Path/Row 14/34, 14/33, 13/32, 13/31, 14/32, and 14/35. The selection and filtering resulted in a variable number of scenes per pixel across the study sites, e.g. the pixel in the Southern Long Island study area had 144 scenes (Fig 2). The average number of scenes after filtering for each watershed was 173.5, 173.0, 139.5, 169.7, 141.5, 146.3, and 170.2 for the Eastern Lower Delmarva, Tangier, Southern Long Island, Chincoteague, Mullica-Toms, Great Egg Harbor, and Albemarle, respectively. GEE was used to convert Landsat 7 surface reflectance to Landsat 8 surface reflectance following the methods in [42]. The transformed values were then used to calculate vegetation indices, Wide Dynamic Range Vegetation Index (WDRVI), Soil Adjusted Vegetation Index (SAVI), Normalized Difference Red Green, Normalized Difference Green Blue, Normalized Difference SWIR2 Red, Normalized Difference SWIR2 NIR, Normalized Difference Water Index_{green, swir} (NDWI_{green, swir}), and NDWI_{nir, swir} utilized in the tidal filtering and random forest regression estimating AGB [43]. Raw time series of the spectral indices were computed for each pixel within the defined extent of salt marsh and exported from GEE (Fig 3).

National Wetland Inventory (NWI) data were used to select all pixels within the estuarine emergent vegetation class. The use of the NWI to constrain the analysis ensured that biomass

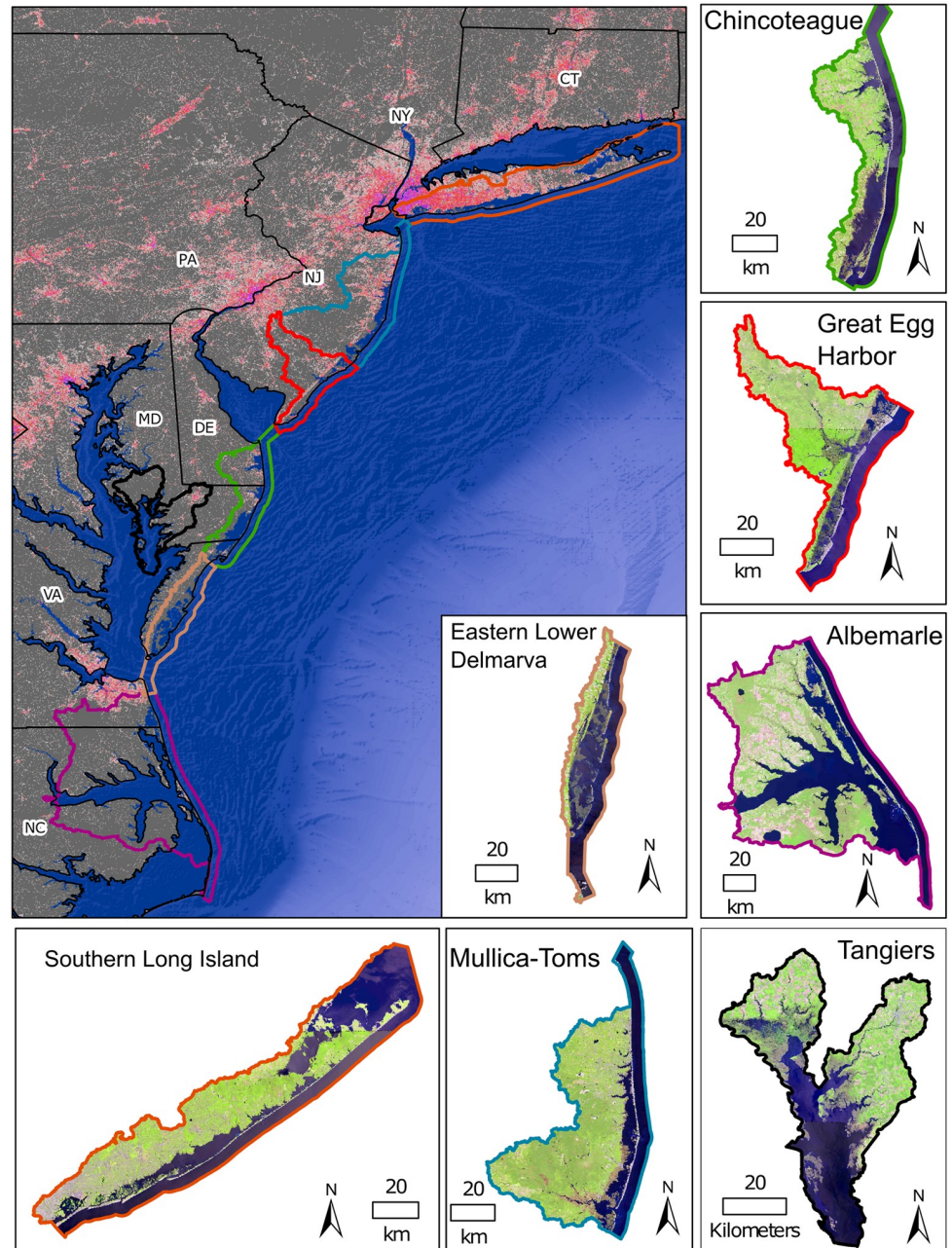


Fig 1. The seven HUC-8 watersheds located across the mid-Atlantic coast. Background data in display are 100 m impervious surface [40] and 30 arc-second GEBCO bathymetry data [41]. Watershed subsets are true color displays of the Landsat 8 imagery courtesy of the U.S. Geological Survey with HUC-12 watershed outlines in grey. Color outlines match watersheds in the overview to each watershed inset.

<https://doi.org/10.1371/journal.pone.0229605.g001>

models were applied to only salt marsh pixels. Pixel centroids which fell directly within creeks, ditches, and mapped pools were also excluded, resulting in the removal of some partial salt marsh pixels from the analysis. Some concern surrounds the use of the NWI layers e.g. an Illinois field assessment found they omit many wetlands [44]. All of our study areas have been updated since being mapped in the 1970/1980s, and had image acquisition dates between

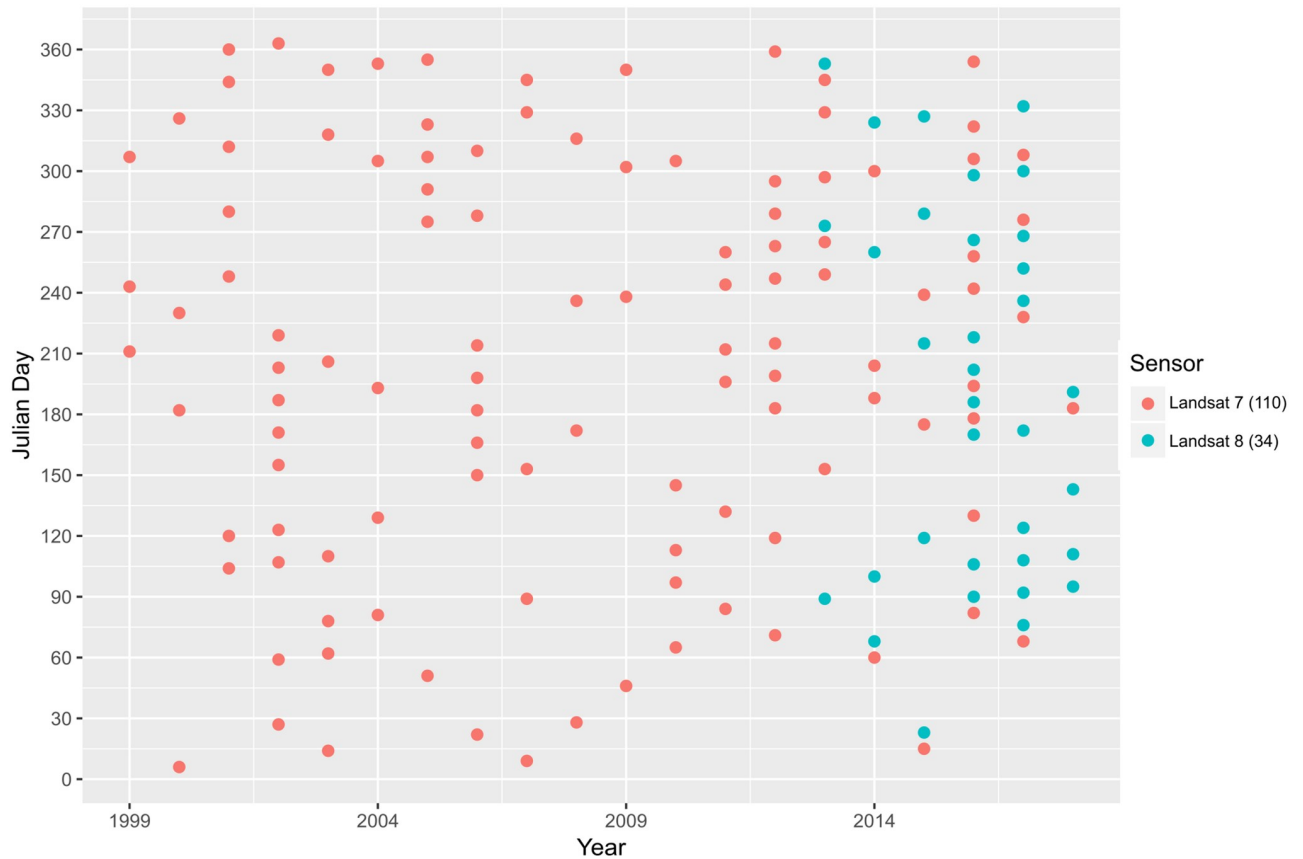


Fig 2. The year, Julian date, and Landsat sensor of each image after filtering by pixel cloud cover and TMII for a single Southern Long Island watershed time series.

<https://doi.org/10.1371/journal.pone.0229605.g002>

2000–2015. The exception being the Albemarle watershed which had a range of image dates between 1977–2015, however, salt marshes were only in areas mapped between 1990–2015. A linear regression model was used to compare image acquisition date and average within watershed change rates.

VHR satellite imagery, e.g., Worldview-2 data, were used to verify the relationship of AGB estimates and vegetation extent. The Worldview-2 data were collected on October 11 and October 16, 2016, for the Chincoteague watershed. This imagery covered the entirety of Assateague Island. Multispectral Worldview-2 imagery possesses 2.4 m spatial resolution and a panchromatic band of 0.46 m. The spectral coverage includes 8 bands ranging from coastal blue, blue, green, yellow, red, red edge, to near infrared.

Landsat tidal marsh inundation index

Many spectral indices such as the Enhanced Vegetation Index share formulas between Landsat and MODIS. TMII was developed for MODIS data. This study assessed the index for use with Landsat data. $NDWI_{green, swir}$ and $NDWI_{nir, swir}$ were calculated for each salt marsh pixel. The $NDWI_{nir, swir}$ was averaged for each month across each pixel's time series for a single sensor. The monthly mean replaced the rolling average of the MODIS TMII which included 44 temporally adjacent images [34]. Replicating such a rolling average would not be reasonable for

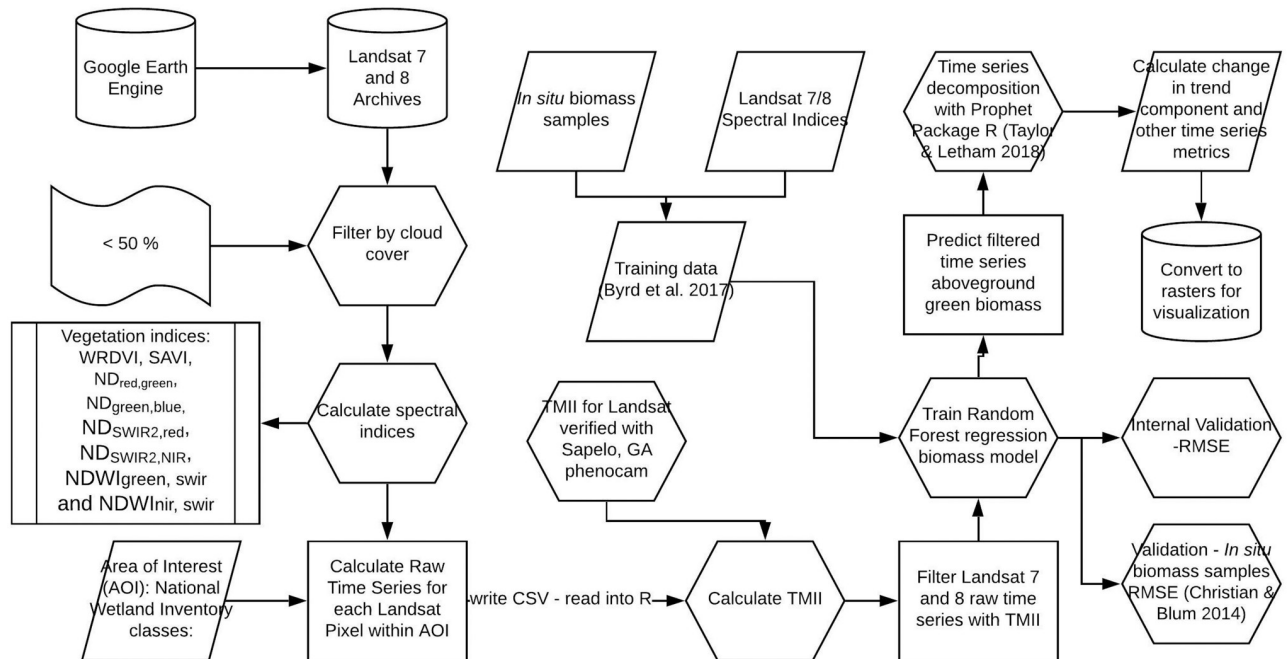


Fig 3. Diagram of the study's GEE data processing, AGB model, verification, and time series analysis.

<https://doi.org/10.1371/journal.pone.0229605.g003>

our coarse temporal resolution. The adapted formulas and the original MODIS formulation are shown below.

1. MODIS TMII (Eq 1)

$$TMII = (1 - (1/e^{(0.3 + 16.6 * NDWI_{4,6} - 25.2 * \text{rolling mean}(NDWI_{2,5})))) \quad (1)$$

[34].

2. Landsat 7 TMII (Eq 2)

$$TMII = (1 - (1/e^{(0.3 + 16.6 * NDWI_{2,5} - 25.2 * \text{monthly mean}(NDWI_{4,5})))) \quad (2)$$

3. Landsat 8 TMII (Eq 3)

$$TMII = (1 - (1/e^{(0.3 + 16.6 * NDWI_{3,6} - 25.2 * \text{monthly mean}(NDWI_{5,6})))) \quad (3)$$

The resulting index was evaluated at the Sapelo Island, GA phenocam across Landsat 7 and Landsat 8 images from WRS-2 Path/Row 16/38 and 17/38 and a date range from 8/09/2013 to 5/03/2018. The evaluation followed the approach of [34] i.e. verifying if the salt marsh visible from the phenocam was inundated or not during a Landsat image acquisition.

Above ground biomass model

Vegetation indices are frequently used in time series analysis, including monitoring forest disturbance [45], rice distribution [46], agricultural abandonment [47], and salt marsh change [48]. NDVI and many related vegetation indices (i.e. WRDVI and SAVI) are indicators of aboveground biomass [49]. Recent methods for estimating AGB in freshwater and salt marsh

environments have relied on vegetation indices [43,50]. This method allows for the estimation of AGB for the majority of plants common in the estuarine emergent wetland category of [51]. By utilizing AGB instead of vegetation indices this study seeks to communicate to a wider interdisciplinary audience.

The spectral indices were converted to AGB following the methods put forth in [43] which achieved a RMSE of 310 g/m² and R² = 0.59, for calculating AGB with Landsat data. A training data set of *in situ* biomass and corresponding Landsat spectral indices (n = 2400) were collected from 2005 to 2015 in San Francisco Bay, the Everglades, Louisiana, Cape Cod, Puget Sound, and Chesapeake [52]. A random forest model was trained utilizing a subset of the training data to control for over representation of the San Francisco Bay and Everglades training points [43]. This study trained a model following the same approach and achieving similar results, however, given the random downsampling model performance varied slightly.

Further verification of the model was performed using end of season *in situ* biomass estimates from 1999–2014 for the Eastern Lower Delmarva and Chincoteague Watersheds [53]. These samples were outside the area previously sampled and represent the transferability of the model to the additional watersheds. The aboveground biomass estimates included 16 sites at Mill Creek, Bellvue, Steelman's landing, Gator Track, Cushman's landing, Oyster Marsh, Indian Town, Box Tree, Brownsville, Hog Island north, Hog Island south, Kegotank, Green Creek, Wallops Island, Woodland Farm, and Assateague [53]. The sites were sampled along transects at four locations, creekside, low marsh, high marsh, and upland transition [53]. Replicates from each location were averaged to get an estimate of each sites aboveground biomass in a single year which was then compared to the average AGB estimates for July, August, and September in the corresponding years. RMSE was calculated considering each year at each site, and comparing the average across all years for each site.

Time series analysis and statistical analysis

The time series analysis was conducted on Landsat 7 and 8 scenes filtered by cloud cover <50%, pixel quality, and a TMII value of >0.2. Landsat 5 data were not utilized in this study due to the lack of both a conversion method into Landsat 8 surface reflectance and verification of the AGB model [42, 43].

The R package Prophet was used for time series analysis [54]. The seasonal-trend decomposition method uses locally weighted regression smoother (LOESS) to isolate the seasonality, trend, and noise [55]. The approach has been used for many remote sensing time series studies [30,35,56]. The prophet package was used due to its robustness to irregular time series, ability to calculate many time series and identify trends and seasonality. All measures of change were derived from the time series analysis using the trend component i.e. trend end–trend start resulting in time series derived measure of change in AGB.

The effect of tidal range on salt marsh change was explored with the use of data from NOAA tidal stations. The tidal ranges of each tidal station within the study area were interpolated into a raster map of tidal ranges as they coincided with HUC-12 watersheds within the study area (Fig 1). All Landsat centroids that were in the interior of the salt marsh, i.e., >30 m from an edge, were analyzed. The effect of tidal range on average change in AGB across HUC-12 watersheds for the four most prevalent salt marsh classes, i.e., *estuarine emergent regularly flooded*, *estuarine emergent irregularly flooded*, *estuarine emergent ditched regularly flooded*, and *estuarine emergent ditched irregularly flooded*, were compared with linear regression. The average change in AGB was compared to the average tidal range. The Albemarle watershed, NC was excluded from the analysis due to the large gaps between tidal stations. Each HUC-12 watershed also had the change rate for edge pixels and interior pixels compared. Edge pixels

were those within 20 m of the NWI polygon boundary. Interior pixels were those further than 20 m from the NWI polygon boundary.

An analysis of all Landsat pixels of the *estuarine emergent regularly flooded*, *estuarine emergent irregularly flooded*, *estuarine emergent ditched regularly flooded*, and *estuarine emergent ditched irregularly flooded* classes were conducted for each HUC-8 watershed. Kruskal-Wallis and post-hoc Dunn's test with Bonferroni adjustment compared the trend in AGB from 1999 to 2018 for each watershed across these four salt marsh classes. Kruskal-Wallis is a non-parametric comparison on ranks [57], pairwise comparisons between classes were conducted using Dunn's test [58].

Worldview-2 image classification of interior salt marsh mudflats was used to assess the relationship of AGB estimates and vegetation extent within the test pixel. The Worldview-2 image classification was an object-based image analysis [14,21]. This analysis was conducted for a portion of the salt marsh on the Maryland side of Assateague Island within the Chincoteague watershed. This analysis was conducted for mudflats on Assateague Island which corresponded with WRS-2 Path/Row 14/33.

Results

Tidal marsh inundation index

The TMII was assessed by evaluating the inundation of each Landsat image date and time of collection at the phenocam and by plotting the decomposed time series before and after filtering (Fig 4). The filtered time series removed all pixels with a TMII >0.2. This level of TMII was suggested previously and performed well in the analysis with the phenocam. The filtered time series removed extreme outliers reduced the observed trend and improved the seasonal graph. The phenocam analysis had a limited number of inundated scenes to work with using images from both WRS-2 Path/Row 16/38 and 17/38. For Landsat 7 and 8, the phenocam image evaluation verified that 10 of the 14 images with TMII >0.2 were inundated. The performance improved slightly when just considering the Landsat 8 imagery, which found 7 out of 9 inundated images were correctly identified. The index had few false negatives for inundation with 148 out of 150 non-inundated images being accurately determined. The filter was applied due to its ability to remove outliers and improve both the seasonal and trend component of the time series decomposition (Fig 4).

Biomass model and change

The ability of the time series trend component to reveal salt marsh change was evident in the identification of both losses and gains across the watersheds. Across the studied watersheds 52% of salt marsh experienced a decline in AGB with an average change of -17 g/m^2 (Table 1).

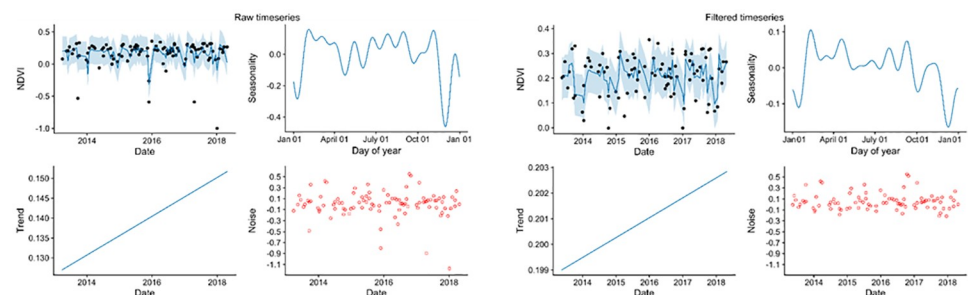


Fig 4. Evaluation of TMII with time series analysis using Landsat 7 and 8. Raw time series includes inundated dates. Filtered time series was excluded dates with TMII > 0.2.

<https://doi.org/10.1371/journal.pone.0229605.g004>

Table 1. The percentage of change, total area, and mean trend of estuarine emergent irregularly flooded, estuarine emergent regularly flooded, estuarine emergent irregularly flooded ditched, and estuarine emergent regularly flooded ditched classes from 1999 to 2018.

HUC 8 Code	Name	Decrease (%)	Increase (%)	Area (hectares)	Mean trend (g/m ²)
02080110	Tangier	35	65	35650	15
02030202	Southern Long Island	76	24	7226	-48
02040301	Mullica-Toms	48	52	18891	1
02040302	Great Egg Harbor	49	51	21172	3
02040303	Chincoteague	62	38	14538	-63
02040304	Eastern Lower Delmarva	75	25	25880	-67
03010205	Albemarle	40	60	16223	5
	Mid-Atlantic coast	52	48	139580	-17

<https://doi.org/10.1371/journal.pone.0229605.t001>

In the Chincoteague watershed, declines were common, and interior loss along the back-barrier of Assateague Island National Seashore was apparent (Fig 5). Increases in AGB were most prominent in the prograding areas to the south of Assateague Island (Fig 5c) and on the overwash fans on northern Assateague Island (Fig 5b). Chincoteague, Eastern Lower Delmarva,

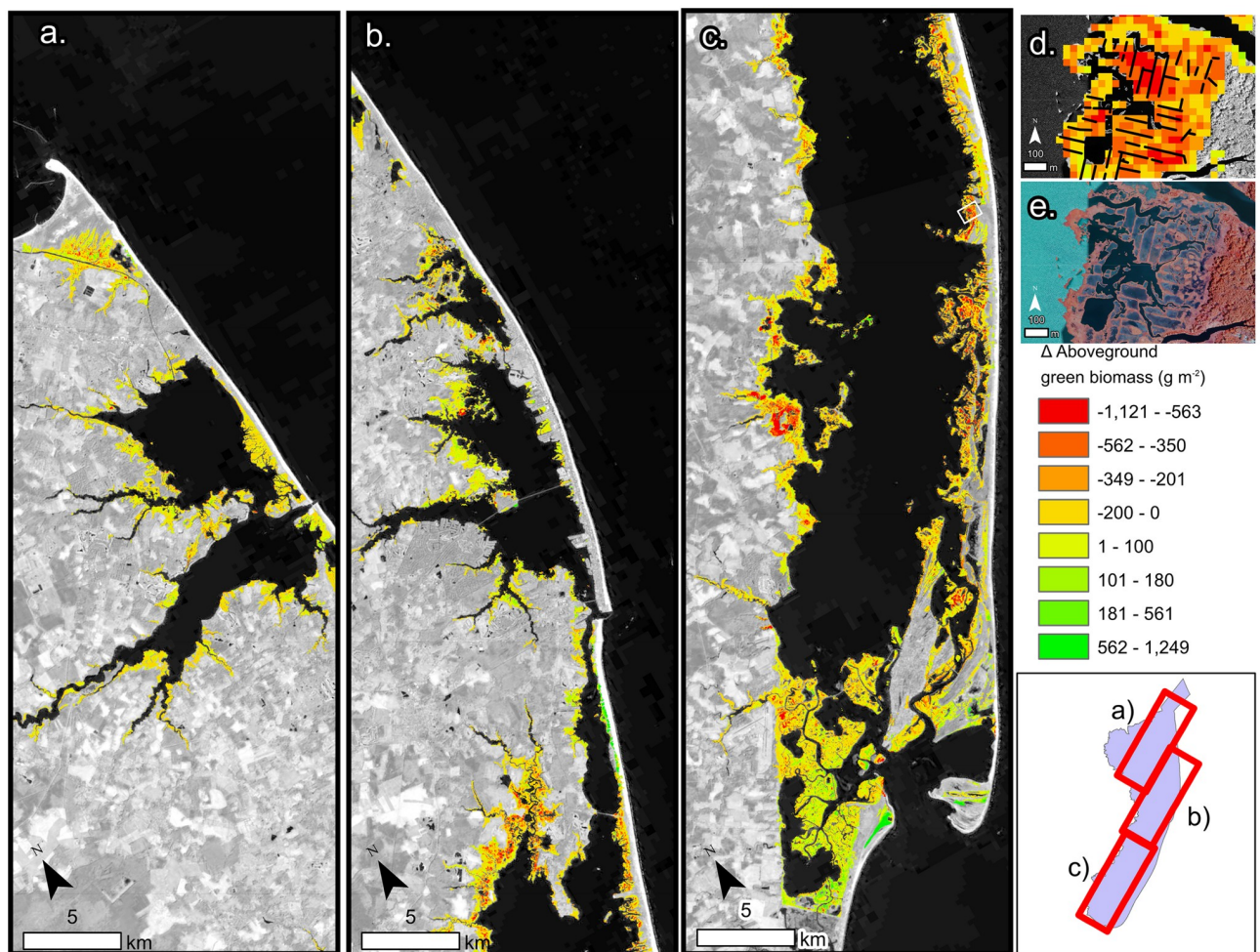


Fig 5. a-c. Change in AGB from 1999–2018 for the Chincoteague watershed, encompassing the eastern shore of Maryland and a section of Virginia and Delaware. Background image Landsat 8 courtesy of the U.S. Geological Survey d. Inset (white box in c.) of salt marsh change and mosquito ditches. e. 2018 NAIP imagery courtesy of the U.S. Geological Survey in pseudo-color image of the same extent as d.

<https://doi.org/10.1371/journal.pone.0229605.g005>

and Southern Long Island all had moderate declines in biomass (Table 1). Tangiers, Mullica-Toms, Albemarle, and Great Egg Harbor had slight increases. The Chincoteague, Eastern Lower Delmarva, and Southern Long Island watersheds demonstrated considerable net loss of AGB (Fig 6). The Eastern Lower Delmarva watershed had the largest average loss which was -67 g/m^2 . The Tangier watershed had the largest average gain which was 15 g/m^2 .

The *in situ* analysis resulted in a site-wide RMSE of $144 \pm 7 \text{ g/m}^2$ with the confidence interval resulting in a conversion factor from wet biomass to dry of between 0.55 and 0.6. The *in situ* yearly RMSE for the Eastern Lower Delmarva watershed 1999 to 2014 was found to be $298 \text{ g/m}^2 \pm 15$. This RMSE compares favorably with the RMSE calculated internally 310 g/m^2 [43], and arrived at by this study (RMSE of $350 \text{ g/m}^2 \pm 16$, $R^2 = 0.62$). The areas of uncertainty include the exact location of the sampling sites and differences between dates of the end of season sampling and July, August, and September satellite estimates.

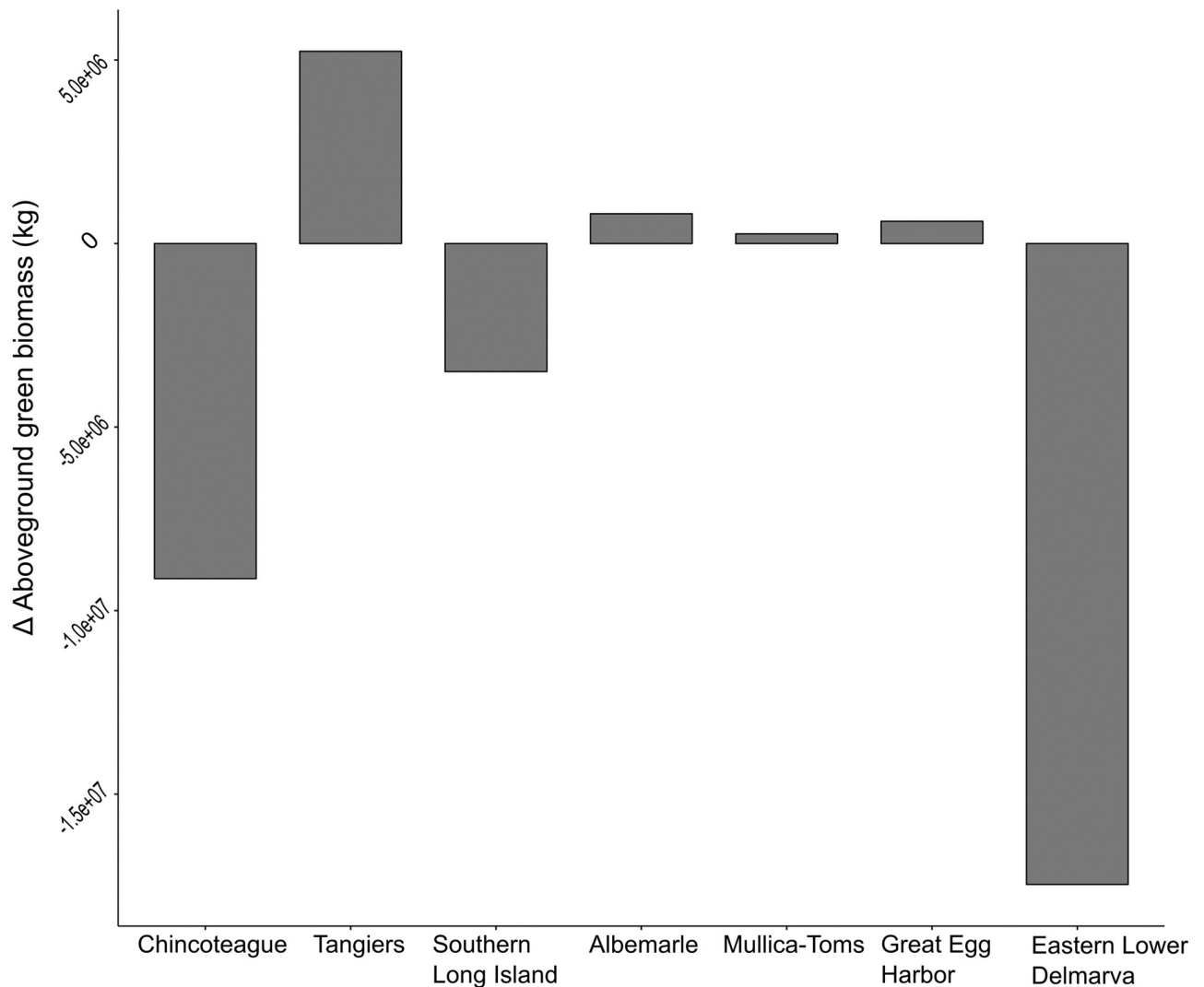


Fig 6. The net change (1999–2018) in AGB for each watershed.

<https://doi.org/10.1371/journal.pone.0229605.g006>

Time series trend and statistical analysis

The NWI acquisition dates effect on change rate for the area was determined across all watersheds. No relationship between acquisition date and change rate was found ($F_{(1,18)} = 0.67$, $p = 0.42$) and $R^2 = -0.02$. Instead the rates of change varied greatly both across watersheds and within a watershed. The analysis with Moran's I for each of the watershed confirmed clustering of salt marsh change within all watersheds (Table 2). In particular, the Eastern Lower Delmarva watershed, which had the largest total loss, has very evident clusters of loss (Figs 6 and 7). Trend maps reveal a clustering of loss around landscape features such as ditches, inlets, and rivers even in stable watersheds (Fig 8).

Kruskal-Wallis test was used to test the difference between dominant salt marsh types with each analysis finding significant differences (Table 3). Dunn's *post hoc* test determined that Chincoteague and Albemarle were the only watersheds were ditched regularly flooded marshes lost vegetation at a lesser rate than regularly flooded salt marshes. Eastern Lower Delmarva and Tangiers were the watersheds where the regularly flooded salt marsh lost more biomass than the irregularly flooded salt marsh. Mullica-Toms, Great Egg Harbor, and Tangier watersheds were the watersheds to demonstrate a small increase in AGB. These watersheds were mosaics composed of a combination of increases and decreases in AGB (Figs 8, 9 and 10).

No significant effect of the tidal range was found for the entirety of the average AGB change by HUC-12 watersheds ($F_{(1,573)} = 0.52$, $p = 0.52$) and $R^2 = 0$. However, when comparing those sites with irregular tidal inundation, mosquito ditches, and a tidal range < 0.8 m; then sites with small tidal ranges saw significantly more loss ($F_{(1,34)} = 6.2$, $p < 0.05$) and $R^2 = 0.16$). When comparing those sites with regular tidal inundation, mosquito ditches, and a tidal range < 0.8 m; then small tidal ranges also saw significantly more loss ($F_{(1,14)} = 7.1$, $p < 0.05$) and $R^2 = 0.33$). Neither inundation regime without mosquito ditches had a significant relationship to tidal range.

The relationship of Landsat derived estimates of AGB and salt marsh extent were verified with Worldview-2 image classification of salt marsh on Assateague Island National Seashore [59]. The Worldview-2 classification was used to compare non-vegetated extent within a pixel to the estimates of AGB. This comparison found a negative relationship between biomass estimates and the area of mudflat within a pixel ($F_{(1165,1)} = 1316$, $p < 0.001$) and $R^2 = 0.53$. The verification with VHR imagery suggests that the Landsat AGB is related to vegetation extent.

Discussion

The *in situ* AGB samples from the Eastern Lower Delmarva verify a similar accuracy to internal out-of-box accuracy assessments from the Random Forest model. A RMSE of 310 g/m^2 was achieved in [43] compared to this study's out of box estimate of $350 \pm 16 \text{ g/m}^2$. However,

Table 2. The results of the Moran's I test of spatial autocorrelation for each of the watersheds. The neighbor distance was 200 m across all watersheds.

Watershed	Moran's Index	P value	z-score
Tangier	0.39	< 0.001	1572
Southern Long Island	0.41	< 0.001	1319
Mullica-Toms	0.53	< 0.001	1509
Great Egg Harbor	0.34	< 0.001	1050
Chincoteague	0.57	< 0.001	1252
Eastern Lower Delmarva	0.45	< 0.001	1513
Albemarle	0.41	< 0.001	1319

<https://doi.org/10.1371/journal.pone.0229605.t002>

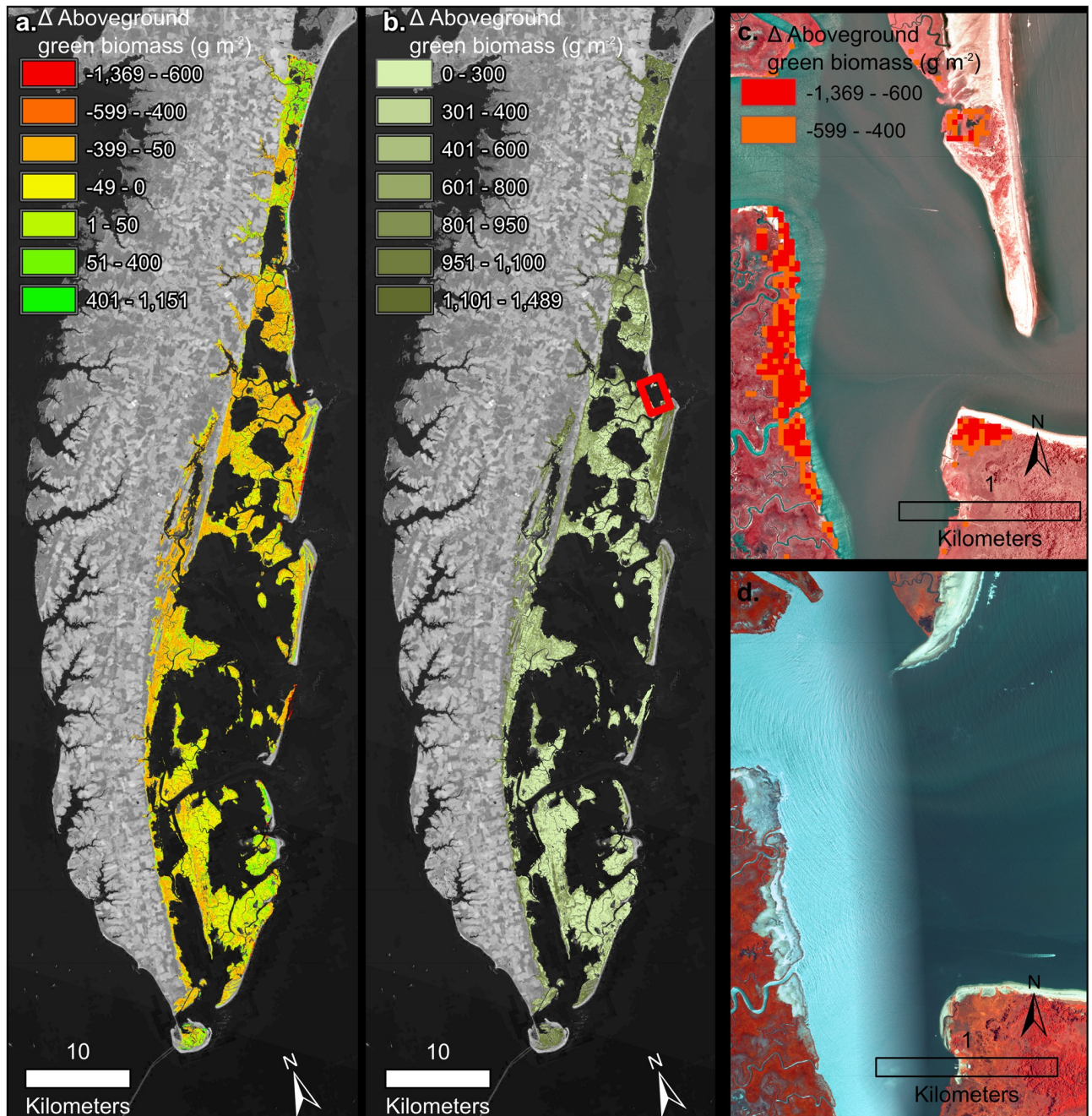


Fig 7. a) Eastern Lower Delmarva watershed change in AGB from 1999 to 2018. b) Eastern Lower Delmarva watershed with the average AGB in July, August, September of 2017. Background imagery Landsat 8 courtesy of U.S. Geological Survey c) Salt marsh trend for an area of loss (2014–2016), NAIP image from 2012 courtesy of the U.S. Geological Survey. d) NAIP 2016 image following barrier spit change.

<https://doi.org/10.1371/journal.pone.0229605.g007>

models have been observed to perform better at the site scale [50]. The site-wide RMSE, compared site averages for all available years, was 144 ± 7 . The yearly comparison between *in situ* samples and Landsat estimates had high variability in part due to different resolutions i.e., *in situ* samples were a much finer resolution (0.0625 m^2) than a Landsat pixel (900 m^2). More *in situ* samples in the site-wide aggregate resulted in an improved RMSE.

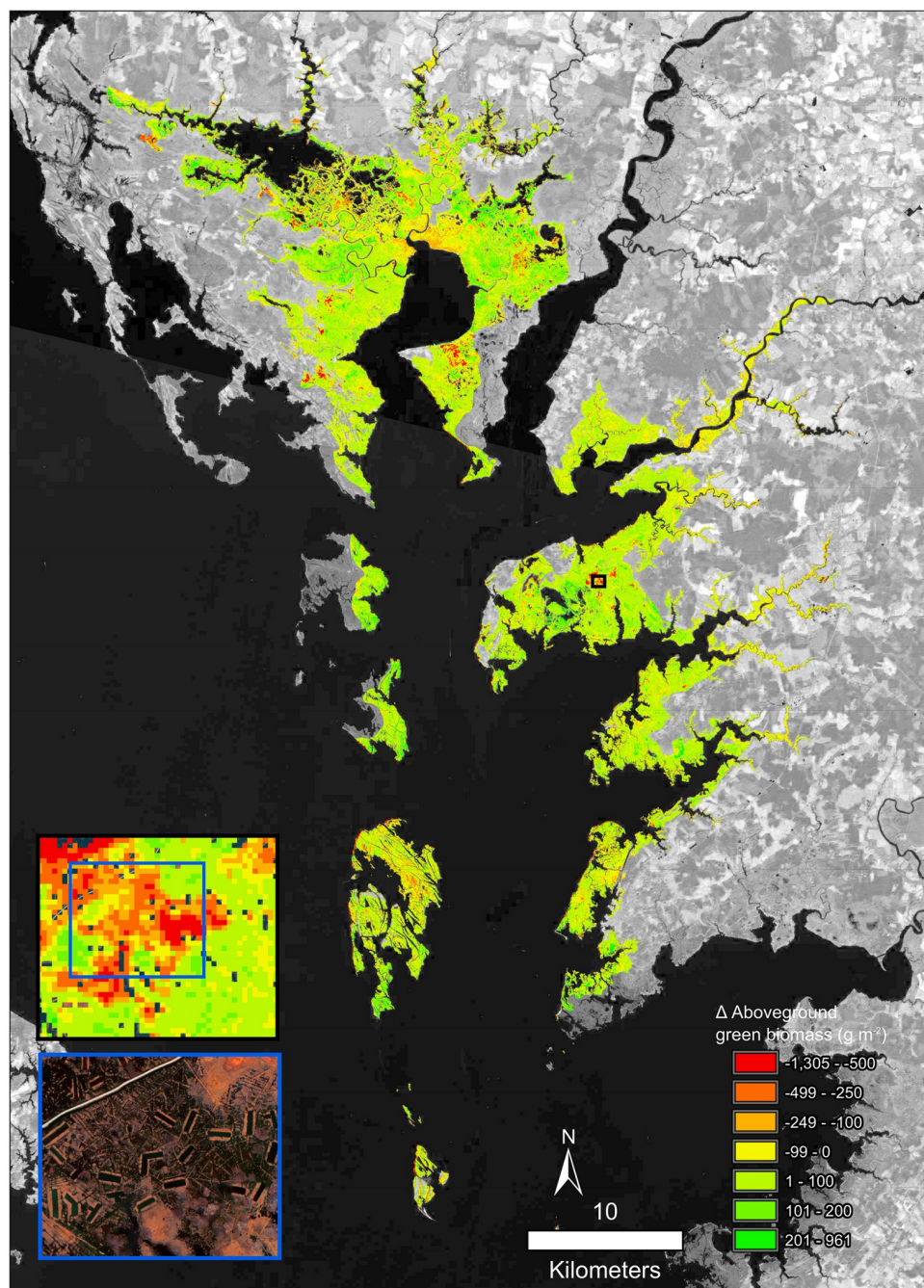


Fig 8. Change in AGB from 1999 to 2018 in the Tangier watershed. a. Shows an inset area of concentrated change in the AGB trend. Background imagery Landsat 8 courtesy of U.S. Geological Survey. b. shows a subset of the heavily ditched area with pseudo color NAIP imagery from 6/1/2017.

<https://doi.org/10.1371/journal.pone.0229605.g008>

AGB loss includes several processes observed in the high-resolution imagery and time series: 1) interior loss and fragmentation, 2) salt marsh loss due to inlet widening and change, 3) edge erosion, and 4) overwash (Fig 11). Additional processes such as the conversion of high marsh to low marsh likely occurred but require additional in situ data to identify. Migration into the upland was outside the scope of this study. However, future studies should pursue monitoring both these components of salt marsh change.

Table 3. The results of the Kruskal-Wallis and Dunn’s post hoc test for each of the 7 watersheds. The tests compared the four most common estuarine emergent vegetation subclasses including irregularly flooded (E2EM1N), regularly flooded (E2EM1P), ditched irregularly flooded (E2EM1Nd), ditched regularly flooded (E2EM1Pd).

Watershed	Kruskal-Wallis	Dunn’s post hoc test					
		regularly flooded vs. ditched regularly flooded	regularly flooded vs. irregularly flooded	ditched regularly flooded vs. irregularly flooded	regularly flooded vs. ditched irregularly flooded	ditched regularly flooded vs. ditched irregularly flooded	irregularly flooded vs. ditched irregularly flooded
Tangier	H(3) = 1239, $p < 0.001$	Z = 11.9 $p < 0.001$	Z = -27.3 $p < 0.001$	Z = -15.4 $p < 0.001$	Z = -16.5 $p < 0.001$	Z = -16.5 $p < 0.001$	Z = -13.9 $p < 0.001$
Southern Long Island	H(3) = 248, $p < 0.001$	Z = 9.0 $p < 0.001$	Z = 8.5 $p < 0.001$	Z = -3.9 $p = 0.001$	Z = 14.4 $p < 0.001$	Z = -0.4 $p = 1.00$	Z = 8.2 $p < 0.001$
Mullica-Toms	H(3) = 3099, $p < 0.001$	Z = 14.5 $p < 0.001$	Z = 2.5 $p = 0.04$	Z = -14.0 $p < 0.001$	Z = 36.9 $p < 0.001$	Z = 5.7 $p < 0.001$	Z = 47.2 $p < 0.001$
Great Egg Harbor	H(3) = 4166, $p < 0.001$	Z = 13.8 $p < 0.001$	Z = 4.1 $p < 0.001$	Z = -12.8 $p < 0.001$	Z = 36.1 $p < 0.001$	Z = 6.1 $p < 0.001$	Z = 57.9 $p < 0.001$
Chincoteague	H(3) = 1280, $p < 0.001$	Z = -5.3 $p < 0.001$	Z = 2.1 $p = 0.1$	Z = 6.8 $p < 0.001$	Z = 28.2 $p < 0.001$	Z = 28.2 $p < 0.001$	Z = 23.4 $p < 0.001$
Eastern Lower Delmarva	H(2) = 2262, $p < 0.001$	NA	Z = -47.5 $p < 0.001$	NA	Z = 2.3 $p = 0.04$	NA	Z = 4.5 $p < 0.001$
Albemarle	H(3) = 2142, $p < 0.001$	Z = -31.6 $p < 0.001$	Z = 14.7 $p < 0.001$	Z = 39.3 $p < 0.001$	Z = 19.9 $p < 0.001$	Z = 43.9 $p < 0.001$	Z = 1.6 $p = 0.36$

<https://doi.org/10.1371/journal.pone.0229605.t003>

AGB declined in three of the study watersheds. Clusters of significant loss were even evident in stable watersheds (Figs 8, 9 and 10). One possible explanation for the variability in watershed-wide change is tidal range. The analysis of tidal range makes it clear that ditched salt marshes with < 0.8 m tidal range were more prone to loss of AGB than the relatively more stable areas (> 0.8 m). This result is supported by previous models which found for the same suspend sediment concentrations macrotidal marshes (>4m tidal range) can adapt to much higher rates of SLR than microtidal (<2 m tidal range) salt marsh [60]. The tidal range and mosquito ditches were some of the site-specific factors which drove loss at the sub-watershed scale. These patterns agree with the literature which suggests long-term declines at the local scale [7,14,15] and projected salt marsh stability until the late 21st century under conservative estimates of SLR [60].

The higher rates of loss in ditched tidal range marshes could be related to the filling of mosquito ditches which has been identified as a possible contributing factor to salt marsh dieback and loss of *Spartina patens* in Rhode Island [61]. The fragility of these microtidal marshes is likely due to the relationship between tidal range and the growth range of *Spartina alterniflora* [62,63]. Ditched salt marshes comprised approximately 1/3 of all salt marsh pixels analyzed. The filling or removal of ditches can result in increased inundation of the salt marsh platform [64]. These salt marshes are undergoing hydrological changes that are altering vegetation extent and quantity of plant biomass.

Edge erosion was compared to interior loss finding all watersheds besides Chincoteague had a higher average rate of edge loss. In Chincoteague watershed edge areas lost on average 56 g/m² compared to interior areas which lost on average 63 g/m². Chincoteague’s site conditions, i.e., microtidal range and mosquito ditches, partially explained the higher rates of loss (Fig 5c; Table 3). Additionally, Chincoteague saw similar rates of loss occurring in regularly flooded and irregularly flooded salt marsh suggesting minimal differences between tidal regimes in microtidal areas (Table 3). However, in both Tangiers and Easter Lower Delmarva regularly flooded salt marsh had a greater loss than an irregularly flooded salt marsh. Despite spatial proximity, these watersheds are experiencing different change regimes.

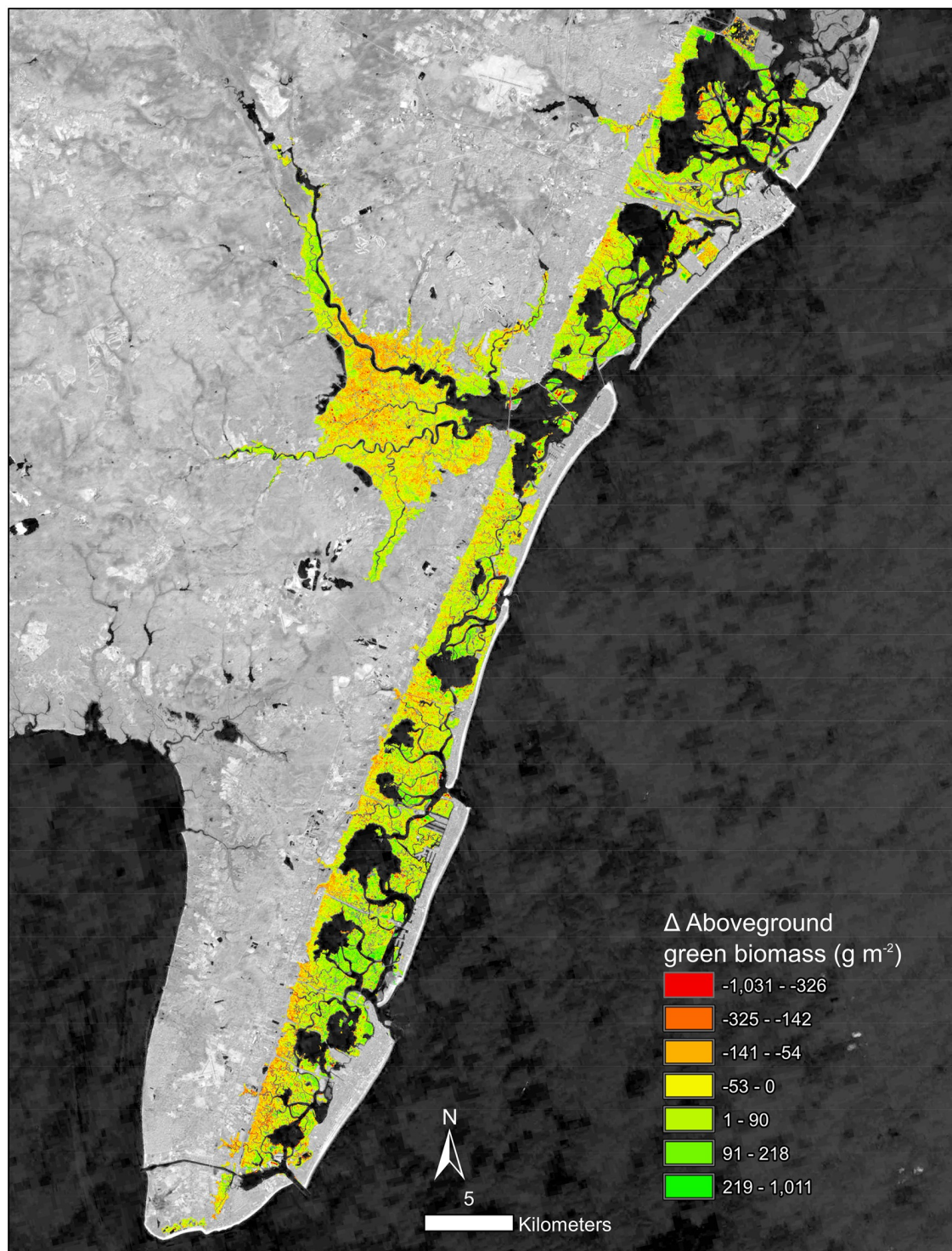


Fig 9. Great Egg Harbor watershed, stretching from Cape May, NJ to just south of Great Bay, NJ. The change of AGB from 1999 to 2018. Background imagery Landsat 8 courtesy of U.S. Geological Survey.

<https://doi.org/10.1371/journal.pone.0229605.g009>

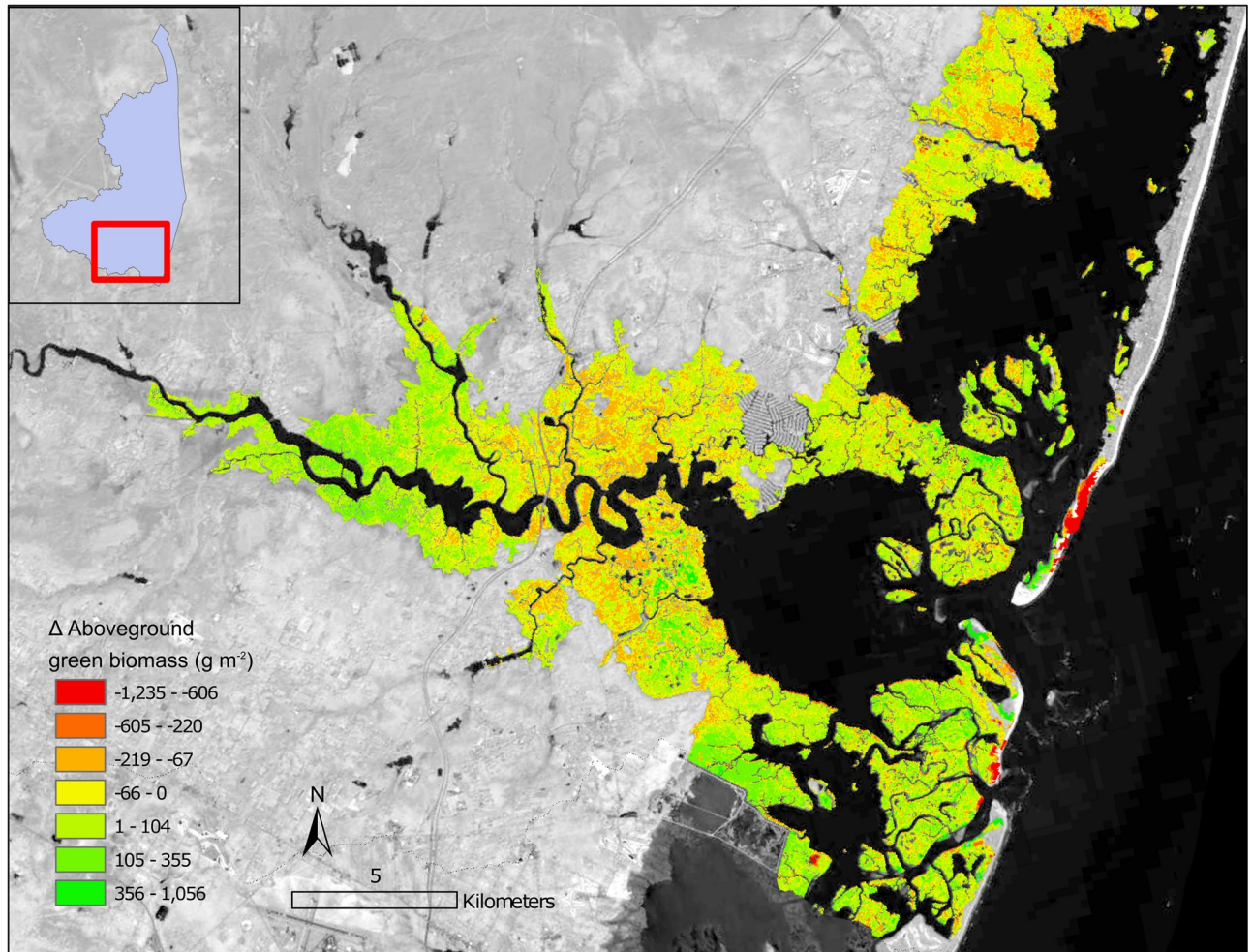


Fig 10. Change in AGB from 1999–2018 for an area surrounding Great Bay, NJ, a section of the Mullica-Toms watershed. Background imagery Landsat 8 courtesy of U.S. Geological Survey.

<https://doi.org/10.1371/journal.pone.0229605.g010>

RMSE was high on individual dates of imagery, decomposing the time series addresses much of this uncertainty by removing both the seasonal component and error isolating the trend, e.g., differencing 2018 AGB by 1999 AGB would compound the error. BFAST, a decomposition-based change detection method was robust to added noise when detecting changes [35]. Additionally, most areas had little change ($< 100 \text{ g/m}^2$) demonstrating the approaches ability to discern stable areas. Small declines in AGB could be the result of within pixel changes, including vegetation type, plant composition, and percent cover or some combination of these factors. For example, increased inundation can cause replacement of high marsh plants with *S. alterniflora*, and this is likely to reduce aboveground biomass [65]. Declines in AGB of irregularly flooded areas were possibly related to the replacement of high marsh with *S. alterniflora* which has been observed on Long Island [66] and Rhode Island [61]. In the mid-Atlantic, estimates of aboveground biomass for *S. patens*, *J. roemerianus*, and *S. alterniflora* were 1399 g/m^2 , 853 g/m^2 , and 257 g/m^2 , respectively [18]. The shift from *S. patens* or *J. roemerianus* to *S. alterniflora* could result in a loss of above, and presumably, belowground biomass.

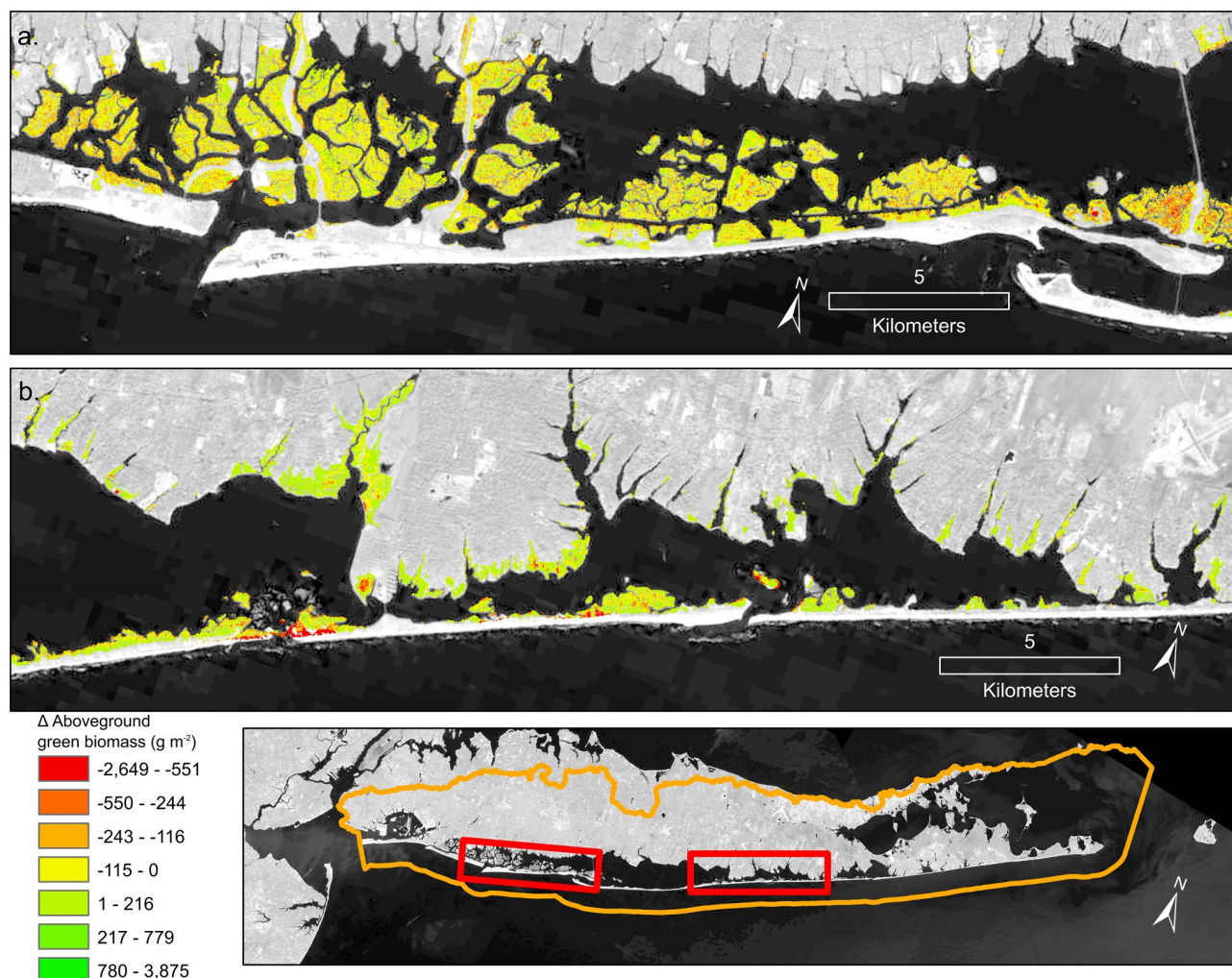


Fig 11. Two subsets of the Southern Long Island watershed. Change in AGB from 1999–2018: a) the back bay salt marshes of Jones Beach Island; b) the north-eastern section of Fire Island and Moriches Bay. Background imagery Landsat 8 courtesy of U.S. Geological Survey.

<https://doi.org/10.1371/journal.pone.0229605.g011>

The high-resolution satellite imagery analysis found that salt marsh/mudflat extent within a pixel partially explained Landsat estimates of AGB. However, vegetation extent did not explain all variation in the AGB. Other likely contributing factors include the amount of water, vegetation composition, and geometric rectification of the two datasets, in some salt marshes *Spartina alterniflora* along the marsh edge has greater aboveground biomass [67]. These differences and other site characteristics result in variability of the biomass estimates. Additional in situ verification would be necessary to establish the relationship of these changes to shifts in the vegetation community.

Tidal filtering

The use of all available data is vital for understanding seasonal and long-term vegetation trends [29]. The time series limited temporal phases due to clouds, tides, 16-day revisit, and Landsat 7's shutter synchronization anomalies makes keeping all quality data essential. The TMII filter is unique to the vegetation cover of a particular pixel. Therefore, it did not over filter those areas with frequent inundation. Adapting the index to Landsat posed several challenges,

including different bandwidths and lower temporal resolution. The conversion of rolling to monthly averages and substitution of bands with appropriate equivalents addressed these issues (Eqs 1–3). The filtering improved time series trend estimates (Fig 4). The rarity of false positives limited any reduction of quality data while removing many inundated images. In this study, the amount of data was essential to ensure enough images were available following filtering by tides, cloud cover, and data quality. Tidal filtering is necessary to improve time series modeling of salt marsh and our understanding of long-term salt marsh change.

Salt marsh change

There is debate about how salt marshes will change in the Anthropocene; site-level research offers conflicting insight into the relationship of SLR to salt marsh loss such as multiple stressors leading to rapid loss [68] or only extreme SLR scenarios (30 cm) resulting in drowning [69]. Modeling studies suggest migration could lead to relative salt marsh stability [16]. Due to differences in scale, these two estimates are not necessarily mutually exclusive, therefore to bridge these studies, we require regional and global studies of salt marsh change such as this one. This study found localized areas of significant salt marsh loss across all watersheds, but also relative stability when examined at the watershed scale. The mid-Atlantic salt marshes are projected to change rapidly, and this research suggests a limited change in many of the watersheds studied. The biomass model utilized in this study should be expanded and verified for additional countries where similar species exist, such as China, where both *Phragmites australis* and *Spartina alterniflora* are prevalent species with a complex relationship [70, 71]. Salt marshes are changing globally [72], with losses resulting in the release of blue carbon stores [73]. A critical carbon sink and potential source are global reasons for interest in salt marsh change. Global studies are not always possible at high spatial resolution and fine time scale. Regional studies in high-risk areas can inform our comprehensive understanding of salt marsh change.

Persistence versus die-off of salt marshes has been attributed to a variety of drivers such as sediment supply [74], edaphic characteristics of the salt marsh [75], elevation [7], nutrient enrichment [4], and basin characteristics [76]. Honeycombing of the interior salt marsh was evident particularly, in ditched salt marshes and across the Chincoteague watersheds (Fig 5d and 5e.). This relationship was most likely due to the combination of altered hydrology from mosquito ditches and small tidal ranges, causing greater vulnerability to SLR. The clustering of change in the salt marsh environments was evident visually and from the results of the Moran's I analysis (Table 1).

The Eastern Lower Delmarva watershed, had a significant average rate of loss (Fig 6) and low average biomass, 529 g/m² over July, August, and September of 2017 (Fig 7b). Barrier island migration at rates of 1–6 m yr⁻¹ drives salt marsh losses in the region [77]. Sediment supply and salt marsh basin width have been suggested as drivers of salt marsh change in the Eastern Lower Delmarva [76]. The Eastern Lower Delmarva represents a different change regime than this study's other barrier island watersheds. Migration of the seaward salt marsh boundary, minor shifts in the interior back-barrier salt marsh, and significant edge erosion due to inlet shifting was evident across the watershed (Fig 7). The time series approach was able to isolate discrete events; however, this process was not automated (Fig 7c). Temporally discrete events such as overwash or barrier spit shifts resulted in a significant reduction in percent AGB for many of the back barrier salt marshes. In the Eastern Lower Delmarva, 1% of all areas analyzed experienced a < -400 g/m² loss from (Summer 2014-Summer 2016). This study demonstrates that the site's salt marshes are low biomass, suggesting even small losses are a

large percent of the sites AGB. This method has the ability to monitor salt marsh under a variety of change regimes.

Conclusion

A combination of medium resolution imagery, time series analysis, biomass modeling, and tidal filtering were utilized to understand salt marsh change. This paper reports a new approach to tidal filtering Landsat time series data for salt marsh environments. The approach improved time series analysis in the tidally inundated areas. The combination of time series analysis and biomass models gave an improved understanding of salt marsh change. The regional study included barrier island ($n = 6$) watersheds across the mid-Atlantic and a sub-watershed of the Chesapeake Bay. AGB declines were identified across the study area, with a mean of -17 g/m^2 (Table 1). In the mid-Atlantic coastal watersheds, 52% of all area analyzed declined from 1999 to 2018. Four watersheds demonstrated positive trends ($> 0 \text{ g/m}^2$), however minor, widespread declines due to SLR were not evident. However, clusters of loss in all watersheds were apparent. These clusters of loss corresponded with barrier island processes and interior drowning.

The methods of this study demonstrate the importance of tidally filtering the time series. Additionally, *in situ* verification of biomass estimates, and use of time series decomposition to isolate long term trends. This study conducted a completely new accuracy assessment from *in situ* data outside the training areas of the biomass models, demonstrating the model's applicability at additional sites in the USA. The conversion to AGB is an important approach for engaging an interdisciplinary audience that may not be familiar with vegetation indices. Further, biomass is a clear indicator of salt marsh resilience, tied to ecogeomorphic feedbacks that contribute to salt marsh resilience. The current analysis demonstrates the use of AGB estimates as an indicator of salt marsh change applied to multiple watershed scales. Limitations of the method lead to the exclusion of important change processes such as migration, future work will include the development of methods to integrate migration into this methodology.

GEE created a single processing environment facilitating the filtering of Landsat images, analysis. The limiting factor for the process was exporting data from GEE to be further analyzed. The Landsat archive is the only option for decadal time series of salt marsh environments with medium spatial resolution and an extensive archive. GEE was an efficient data processing environment for the calculation of vegetation indices, the conversion of Landsat 7 surface reflectance into Landsat 8 surface reflectance, and processing of the raw time series. These methods utilized globally available remote sensing data in the form of the Landsat archive and GEE limiting the computing costs. These methods reduced hardware limitations and expand the potential geographic scope of salt marsh change analysis for both historical assessments and continued monitoring. However, higher spatial resolution imagery, e.g., Sentinel-2, is necessary to increase the sensitivity of this methodology to fine-scale change. Next steps include applying the method to compare a broader range of sites, mapping areas identified as clusters of change with high spatial resolution imagery and expanding the methods to include the long record of Landsat 5 data.

Supporting information

S1 Table. The results of the linear regression analysis for all watersheds aggregated by acquisition date.

(DOCX)

S2 Table. The results of the linear regression analysis for micro tidal areas (< 0.8 m) by vegetation type (E2EM1Nd, E2EM1N, E2EM1P, E2EM1Pd). (DOCX)

Acknowledgments

The authors would like to thank the staff of Jamaica Bay Unit of Gateway National Recreation Area (New York), Fire Island National Seashore, and Assateague National Seashore that assisted with field visits for this project. Thanks to Peter August and Charles Roman who, read and offered feedback on the manuscript.

Author Contributions

Conceptualization: Anthony Daniel Campbell, Yeqiao Wang.

Data curation: Anthony Daniel Campbell.

Formal analysis: Anthony Daniel Campbell.

Funding acquisition: Anthony Daniel Campbell, Yeqiao Wang.

Investigation: Anthony Daniel Campbell.

Methodology: Anthony Daniel Campbell, Yeqiao Wang.

Project administration: Yeqiao Wang.

Resources: Yeqiao Wang.

Supervision: Yeqiao Wang.

Validation: Anthony Daniel Campbell.

Visualization: Anthony Daniel Campbell.

Writing – original draft: Anthony Daniel Campbell.

Writing – review & editing: Anthony Daniel Campbell, Yeqiao Wang.

References

1. Jin Y, Yang W, Sun T, Yang Z, Li M. Effects of seashore reclamation activities on the health of wetland ecosystems: a case study in the Yellow River Delta, China. *Ocean Coast Manage.* 2016; 123: 44–52. Top of FormBottom of Form
2. Saintilan N, Wilson NC, Rogers K, Rajkaran A, Krauss KW. Mangrove expansion and salt marsh decline at mangrove poleward limits. *Global Change Biol.* 2014; 20: 147–157.
3. Armitage AR, Highfield WE, Brody SD, Louchouart P. The contribution of mangrove expansion to salt marsh loss on the Texas Gulf Coast. *PloS one.* 2015; 10: e0125404. <https://doi.org/10.1371/journal.pone.0125404> PMID: 25946132
4. Deegan LA, Johnson DS, Warren RS, Peterson BJ, Fleeger JW, Fagherazzi S, et al. Coastal eutrophication as a driver of salt marsh loss. *Nature.* 2012; 490: 388–392. <https://doi.org/10.1038/nature11533> PMID: 23075989
5. Holdredge C, Bertness MD, Altieri AH. Role of crab herbivory in die-off of New England salt marshes. *Conserv Biol.* 2009; 23: 672–679. <https://doi.org/10.1111/j.1523-1739.2008.01137.x> PMID: 19183205
6. Silliman BR, Zieman JC. Top-down control of *Spartina alterniflora* production by periwinkle grazing in a Virginia salt marsh. *Ecology.* 2001; 82: 2830–2845.
7. Watson EB, Wigand C, Davey EW, Andrews HM, Bishop J, Raposa KB. Wetland Loss Patterns and Inundation-Productivity Relationships Prognosticate Widespread Salt Marsh Loss for Southern New England. *Estuaries and Coasts.* 2017; 40: 662–681. <https://doi.org/10.1007/s12237-016-0069-1> PMID: 30008627

8. Schile LM, Callaway JC, Morris JT, Stralberg D, Parker VT, Kelly M. Modeling tidal marsh distribution with sea-level rise: Evaluating the role of vegetation, sediment, and upland habitat in marsh resiliency. *PLoS one*. 2014; 9: e88760. <https://doi.org/10.1371/journal.pone.0088760> PMID: 24551156
9. Alizad K, Hagen SC, Medeiros SC, Bilskie MV, Morris JT, Balthis L, et al. Dynamic responses and implications to coastal wetlands and the surrounding regions under sea level rise. *PLoS one*. 2018; 13: e0205176. <https://doi.org/10.1371/journal.pone.0205176> PMID: 30312304
10. Crosby SC, Sax DF, Palmer ME, Booth HS, Deegan LA, Bertness MD, et al. Salt marsh persistence is threatened by predicted sea-level rise. *Estuar Coast Shelf Sci*. 2016; 181: 93–99.
11. Boon JD. Evidence of sea level acceleration at US and Canadian tide stations, Atlantic Coast, North America. *J Coast Res*. 2012; 28: 1437–1445.
12. Sweet WV, Kopp RE, Weaver CP, Obeysekera J, Horton RM, Thieler ER, et al. Global and regional sea level rise scenarios for the United States. 2017. NOAA, Silver Spring, MD, USA, Tech. Rep. NOS CO-OPS 083.
13. Dahl TE, Stedman SM. Status and trends of wetlands in the coastal watersheds of the Conterminous United States 2004 to 2009. US Department of the Interior, US Fish and Wildlife Service and National Oceanic and Atmospheric Administration, National Marine Fisheries Service; 2013.
14. Campbell A, Wang Y, Christiano M, Stevens S. Salt marsh monitoring in Jamaica Bay, New York from 2003 to 2013: a decade of change from restoration to Hurricane Sandy. *Remote Sensing*. 2017 Feb 6; 9(2):131.
15. Schepers L, Kirwan M, Guntenspergen G, Temmerman S. Spatio-temporal development of vegetation die-off in a submerging coastal marsh. *Limnol Oceanogr*. 2017; 62: 137–150.
16. Schuerch M, Spencer T, Temmerman S, Kirwan ML, Wolff C, Lincke D, et al. Future response of global coastal wetlands to sea-level rise. *Nature*. 2018; 561: 231. <https://doi.org/10.1038/s41586-018-0476-5> PMID: 30209368
17. Roman CT. Salt marsh sustainability: challenges during an uncertain future. *Estuaries and coasts*. 2017; 40: 711–716.
18. Eelsey-Quirk T, Seliskar DM, Sommerfield CK, Gallagher JL. Salt marsh carbon pool distribution in a mid-Atlantic lagoon, USA: sea level rise implications. *Wetlands*. 2011 Feb 1; 31(1):87–99.
19. Morris JT, Sundareshwar PV, Nietch CT, Kjerfve B, Cahoon DR. Responses of coastal wetlands to rising sea level. *Ecology*. 2002 Oct; 83(10):2869–77.
20. Mudd SM, Fagherazzi S, Morris JT, Furbish DJ. Flow, sedimentation, and biomass production on a vegetated salt marsh in South Carolina: toward a predictive model of marsh morphologic and ecologic evolution. *The Ecogeomorphology of Tidal Marshes, Coastal Estuarine Stud*. 2004 Jan 9; 59:165–87.
21. Campbell A, Wang Y. Examining the influence of tidal stage on salt marsh mapping using high-spatial-resolution satellite remote sensing and topobathymetric lidar. *IEEE Transactions on Geoscience and Remote Sensing*. 2018 Mar 28; 56(9):5169–76. Top of Form
22. Kearney MS, Stevenson JC. Island land loss and marsh vertical accretion rate evidence for historical sea-level changes in Chesapeake Bay. *Journal of Coastal Research*. 1991 Apr 1:403–15.
23. Fu B, Wang Y, Campbell A, Li Y, Zhang B, Yin S, et al. Comparison of object-based and pixel-based Random Forest algorithm for wetland vegetation mapping using high spatial resolution GF-1 and SAR data. *Ecological indicators*. 2017 Feb 1; 73:105–17.
24. Zhao B, Yan Y, Guo H, He M, Gu Y, Li B. Monitoring rapid vegetation succession in estuarine wetland using time series MODIS-based indicators: an application in the Yangtze River Delta area. *Ecol Ind*. 2009; 9: 346–356.
25. Davranche A, Lefebvre G, Poulin B. Wetland monitoring using classification trees and SPOT-5 seasonal time series. *Remote Sens Environ*. 2010; 114: 552–562. <https://doi.org/10.1016/j.rse.2009.10.009>
26. Kayastha N, Thomas V, Galbraith J, Banskota A. Monitoring wetland change using inter-annual landsat time-series data. *Wetlands*. 2012; 32: 1149–1162.
27. O'Donnell J, Schalles J. Examination of abiotic drivers and their influence on *Spartina alterniflora* biomass over a twenty-eight year period using Landsat 5 TM satellite imagery of the Central Georgia Coast. *Remote Sensing*. 2016 Jun; 8(6):477.
28. Hird JN, DeLancey ER, McDermid GJ, Kariyeva J. Google Earth Engine, Open-Access Satellite Data, and Machine Learning in Support of Large-Area Probabilistic Wetland Mapping. *Remote Sensing*. 2017; 9: 1315.
29. Vogelmann JE, Gallant AL, Shi H, Zhu Z. Perspectives on monitoring gradual change across the continuity of Landsat sensors using time-series data. *Remote Sens Environ*. 2016; 185: 258–270.
30. Fu P, Weng Q. A time series analysis of urbanization induced land use and land cover change and its impact on land surface temperature with Landsat imagery. *Remote Sens Environ*. 2016; 175: 205–214.

31. Pasquarella VJ, Holden CE, Kaufman L, Woodcock CE. From imagery to ecology: leveraging time series of all available Landsat observations to map and monitor ecosystem state and dynamics. *Remote Sensing in Ecology and Conservation*. 2016 Sep; 2(3):152–70.
32. Jensen JR, Cowen DJ, Althausen JD, Narumalani S, Weatherbee O. An evaluation of the CoastWatch change detection protocol in South Carolina. *Photogramm Eng Remote Sensing*. 1993; 59: 1039–1044.
33. Basu S, Meckesheimer M. Automatic outlier detection for time series: an application to sensor data. *Knowledge and Information Systems*. 2007; 11: 137–154.
34. O'Connell JL, Mishra DR, Cotten DL, Wang L, Alber M. The Tidal Marsh Inundation Index (TMII): An inundation filter to flag flooded pixels and improve MODIS tidal marsh vegetation time-series analysis. *Remote Sens Environ*. 2017; 201: 34–46.
35. Verbesselt J, Hyndman R, Newnham G, Culvenor D. Detecting trend and seasonal changes in satellite image time series. *Remote Sens Environ*. 2010; 114: 106–115.
36. Weston NB. Declining sediments and rising seas: an unfortunate convergence for tidal wetlands. *Estuaries and Coasts*. 2014; 37: 1–23.
37. Najjar RG, Walker HA, Anderson PJ, Barron EJ, Bord RJ, Gibson JR, et al. The potential impacts of climate change on the mid-Atlantic coastal region. *Climate Research*. 2000 May 2; 14(3):219–33.
38. Crosby SC, Angermeyer A, Adler JM, Bertness MD, Deegan LA, Sibinga N, et al. *Spartina alterniflora* biomass allocation and temperature: implications for salt marsh persistence with sea-level rise. *Estuaries and Coasts*. 2017 Jan 1; 40(1):213–23.
39. Crosby SC, Ivens-Duran M, Bertness MD, Davey E, Deegan LA, Leslie HM. Flowering and biomass allocation in US Atlantic coast *Spartina alterniflora*. *Am J Bot*. 2015; 102: 669–676. <https://doi.org/10.3732/ajb.1400534> PMID: 26022481
40. U.S. Geological Society. 100-Meter Resolution Impervious Surface of the United States. 2013 Mar. https://nationalmap.gov/small_scale/mlid/impe100.html
41. Weatherall P, Marks KM, Jakobsson M, Schmitt T, Tani S, Arndt JE, et al. A new digital bathymetric model of the world's oceans. *Earth and Space Science*. 2015; 2: 331–345.
42. Roy DP, Kovalskyy V, Zhang HK, Vermote EF, Yan L, Kumar SS, et al. Characterization of Landsat-7 to Landsat-8 reflective wavelength and normalized difference vegetation index continuity. *Remote sensing of Environment*. 2016 Nov 1; 185:57–70. <https://doi.org/10.1016/j.rse.2015.12.024> PMID: 32020954
43. Byrd KB, Ballanti L, Thomas N, Nguyen D, Holmquist JR, Simard M, et al. A remote sensing-based model of tidal marsh aboveground carbon stocks for the conterminous United States. *ISPRS Journal of Photogrammetry and Remote Sensing*. 2018; 139: 255–271.
44. Matthews JW, Skultety D, Zercher B, Ward MP, Benson TJ. Field verification of original and updated National Wetlands Inventory maps in three metropolitan areas in Illinois, USA. *Wetlands*. 2016 Dec 1; 36(6):1155–65.
45. DeVries B, Verbesselt J, Kooistra L, Herold M. Robust monitoring of small-scale forest disturbances in a tropical montane forest using Landsat time series. *Remote Sens Environ*. 2015; 161: 107–121.
46. Dong J, Xiao X, Kou W, Qin Y, Zhang G, Li L, et al. Tracking the dynamics of paddy rice planting area in 1986–2010 through time series Landsat images and phenology-based algorithms. *Remote Sensing of Environment*. 2015 Apr 1; 160:99–113.
47. Estel S, Kuemmerle T, Alcántara C, Levers C, Prishchepov A, Hostert P. Mapping farmland abandonment and recultivation across Europe using MODIS NDVI time series. *Remote Sens Environ*. 2015; 163: 312–325.
48. Klemas V. Remote sensing of wetlands: case studies comparing practical techniques. *Journal of Coastal Research*. 2011 Mar 21; 27(3):418–27.
49. Anderson GL, Hanson JD, Haas RH. Evaluating Landsat Thematic Mapper derived vegetation indices for estimating above-ground biomass on semiarid rangelands. *Remote sensing of environment*. 1993 Aug 1; 45(2):165–75.
50. Byrd KB, O'Connell JL, Di Tommaso S, Kelly M. Evaluation of sensor types and environmental controls on mapping biomass of coastal marsh emergent vegetation. *Remote Sens Environ*. 2014; 149: 166–180.
51. Cowardin LM, Carter V, Golet FC, LaRoe ET. Classification of wetlands and deepwater habitats of the United States. *Classification of wetlands and deepwater habitats of the United States*. 1979: 131.
52. Byrd K, Ballanti L, Thomas N, Nguyen D, Holmquist JR, Simard M, et al. Tidal marsh biomass field plot and remote sensing datasets for six regions in the conterminous United States. *US Geol. Surv. Data Release*. 2017; 10: F77943K8.
53. Christian R, and Blum L. End of Year Biomass in Marshes of the Virginia Coast Reserve 1999–2014. *Virginia Coast Reserve Long-Term Ecological Research Project Data 2014*. Publication knb-iter-vcr.167.22

54. Taylor SJ, Letham B. Forecasting at scale. *The American Statistician*. 2017.
55. Cleveland RB, Cleveland WS, McRae JE, Terpenning I. STL: a seasonal-trend decomposition. *Journal of official statistics*. 1990; 6(1):3–73.
56. Zhu Z, Fu Y, Woodcock CE, Olofsson P, Vogelmann JE, Holden C, et al. Including land cover change in analysis of greenness trends using all available Landsat 5, 7, and 8 images: A case study from Guangzhou, China (2000–2014). *Remote Sens Environ*. 2016; 185: 243–257.
57. Kruskal WH, Wallis WA. Use of ranks in one-criterion variance analysis. *Journal of the American statistical Association*. 1952 Dec 1; 47(260):583–621.
58. Dunn OJ. Multiple comparisons using rank sums. *Technometrics*. 1964 Aug 1; 6(3):241–52.
59. Wang YQ, and Campbell A. Monitoring salt marshes using high spatial resolution satellite imagery for mapping and change detection: Protocol development for northeast coastal parks. 2018. Natural Resource Report NPS/NCBN/NRR—2018/1717. National Park Service, Fort Collins, Colorado.
60. Kirwan ML, Guntenspergen GR, d'Alpaos A, Morris JT, Mudd SM, Temmerman S. Limits on the adaptability of coastal marshes to rising sea level. *Geophys Res Lett*. 2010; 37.
61. Raposa KB, Weber RL, Ekberg MC, Ferguson W. Vegetation dynamics in Rhode Island salt marshes during a period of accelerating sea level rise and extreme sea level events. *Estuaries and Coasts*. 2017 May 1; 40(3):640–50.
62. Mckee KL, Patrick WH. The relationship of smooth cordgrass (*Spartina alterniflora*) to tidal datums: a review. *Estuaries*. 1988; 11: 143–151.
63. Cahoon DR, Lynch JC, Roman CT, Schmit JP, Skidde DE. Evaluating the Relationship Among Wetland Vertical Development, Elevation Capital, Sea-Level Rise, and Tidal Marsh Sustainability. *Estuaries and Coasts*: 1–15.
64. Corman SS, Roman CT, King JW, Appleby PG. Salt marsh mosquito-control ditches: sedimentation, landscape change, and restoration implications. *J Coast Res*. 2012; 28: 874–880.
65. Snedden GA, Cretini K, Patton B. Inundation and salinity impacts to above-and belowground productivity in *Spartina patens* and *Spartina alterniflora* in the Mississippi River deltaic plain: Implications for using river diversions as restoration tools. *Ecol Eng*. 2015; 81: 133–139.
66. Cameron Engineering and Associates. Long Island tidal wetlands trends analysis. New England Interstate Water Pollution Control Commission, 2015 1: 207.
67. Dame RF, Kenny PD. Variability of *Spartina alterniflora* primary production in the euhaline North Inlet estuary. *Marine Ecology Progress Series*. 1986 Aug 14:71–80.
68. Crotty SM, Angelini C, Bertness MD. Multiple stressors and the potential for synergistic loss of New England salt marshes. *PloS one*. 2017; 12: e0183058. <https://doi.org/10.1371/journal.pone.0183058> PMID: 28859097
69. Nelson JL, Zavaleta ES. Salt marsh as a coastal filter for the oceans: changes in function with experimental increases in nitrogen loading and sea-level rise. *PLoS One*. 2012; 7: e38558. <https://doi.org/10.1371/journal.pone.0038558> PMID: 22879873
70. Yuan Y, Wang K, Li D, Pan Y, Lv Y, Zhao M, et al. Interspecific interactions between *Phragmites australis* and *Spartina alterniflora* along a tidal gradient in the Dongtan Wetland, Eastern China. *PloS one*. 2013; 8: e53843. <https://doi.org/10.1371/journal.pone.0053843> PMID: 23342017
71. Liu M, Mao D, Wang Z, Li L, Man W, Jia M, et al. Rapid invasion of *Spartina alterniflora* in the coastal zone of mainland China: New observations from Landsat OLI images. *Remote Sensing*. 2018; 10: 1933.
72. Simas T, Nunes JP, Ferreira JG. Effects of global climate change on coastal salt marshes. *Ecol Model*. 2001; 139: 1–15.
73. Macreadie PI, Hughes AR, Kimbro DL. Loss of 'blue carbon' from coastal salt marshes following habitat disturbance. *PloS one*. 2013; 8: e69244. <https://doi.org/10.1371/journal.pone.0069244> PMID: 23861964
74. Anisfeld SC, Cooper KR, Kemp AC. Upslope development of a tidal marsh as a function of upland land use. *Global change biology*. 2017 Feb; 23(2):755–66. <https://doi.org/10.1111/gcb.13398> PMID: 27343840
75. Crawford JT, Stone AG. Relationships between soil composition and *Spartina alterniflora* dieback in an Atlantic salt marsh. *Wetlands*. 2015 Feb 1; 35(1):13–20.
76. Mariotti G, Fagherazzi S. Critical width of tidal flats triggers marsh collapse in the absence of sea-level rise. *Proceedings of the National Academy of Sciences*. 2013; 110: 5353–5356.
77. Deaton CD, Hein CJ, Kirwan ML. Barrier island migration dominates ecogeomorphic feedbacks and drives salt marsh loss along the Virginia Atlantic Coast, USA. *Geology*. 2017; 45: 123–126.